Extreme Dry and Wet Events in Iceland: Observations, Simulations and Scenarios

FRANK SIENZ[1], ISABELLA BORDI[2], KLAUS FRAEDRICH[1] AND ANDREA SCHNEIDEREIT[1]

[1]Universität Hamburg, Meteorologisches Institut, Bundesstraße 55, D-20146 Hamburg
[2]Universita degli Studi di Roma "La Sapienza", Dipartimento di Fisica, Piazzale Aldo Moro 2, I-00185 Roma

(Manuscript received Month DD, YYYY; in revised form Month DD, YYYY; accepted Month DD, YYYY)

Abstract

Monthly extremes of dryness and wetness in Iceland are analysed based on the standardised precipitation index (SPI). The analysis is performed for observations and four sets of coupled atmosphere-ocean climate model simulations (ECHAM5/MPI-OM) to link water cycle extremes in Iceland with regional atmospheric flow patterns and to estimate and evaluate future changes. The following results are obtained: (i) SPI extremes are linked with a Europe-Greenland Index (EGI) describing south-westerly flow anomalies by a dipole and the related geopotential height differences. The good agreement between the observed statistics and transient 20th century simulations encourages analysis of future climate projections. (ii) Comparison of the 21st century A1B-scenario with the pre-industrial climate reveals significant and large differences: While extremes of dryness hardly change, extremely wet conditions increase in winter and spring. As there is no flow intensification and cyclone density decreases, the cause maybe found air moisture raising in a warmer climate.

Zusammenfassung

Extreme trockene und nasse Ereignisse in Island: Beobachtungen, Simulationen und Szenarien

Monatliche Extreme von Trockenheit und Nässe in Island werden mit Hilfe des "standardised precipitation index" (SPI) analysiert. Untersucht werden Beobachtungen und vier verschiedene Klimasimulationen eines gekoppelten Atmosphären-Ozean Modells (ECHAM5/MPI-OM), um Extreme im Wasserkreislauf von Island mit regionalen atmophärischen Strömungsmustern in Zusammenhang zu bringen, sowie zur Bestimmung und Bewertung zukünftiger Änderungen. Die folgenden Ergebnisse werden erhalten: (i) SPI Extreme sind mit einem Europa-Grönland Index (EGI) verbunden, der südwestliche Strömungsanomalien durch einen Dipol mit den dazu gehörigen geopotentiellen Höhendifferenzen beschreibt. Die gute Übereinstimmung zwischen beobachteter Statistik und transienten Simulationen des 20. Jahrhunderts unterstützt die Untersuchung zukünftiger Klimaprojektionen. (ii) Der Vergleich zwischen dem A1B-Szenario des 21. Jahrhunderts und dem vorindustriellen Klima zeigt große und signifikante Unterschiede: Obwohl sich extreme Trockenheiten kaum ändern, nehmen extrem nasse Bedingungen in Winter und Frühjahr zu. Diese sind nicht ein Ergebnis sich intensivierender Zirkulationsanomalien, sondern ergeben sich möglicherweise aus einer Erhöhung der Luftfeuchtigkeit in einem wärmeren Klima, zumal auch die Zyklonenzahldichte sich verringert. Die saisonal unterschiedlichen Reaktionen der Klimaänderung stehen jedoch im Zusammenhang mit Änderungen der Strömungsmuster.

1 Introduction

Iceland's climate and climate variability are commonly associated with stormtracks and cyclone path regimes (SCHNEIDEREIT et al. (2007)) depending on teleconnections affecting the North Atlantic sector like, for example, the North Atlantic Oscillation (NAO) or El Nino - Southern Oscillation (ENSO); for comprehensive reviews see SFB-512 (2005) and FRAEDRICH (1994). Here, however, the indicator of climate variability to be analysed is not the meridional surface pressure dipole between Iceland and the Azores, but extremes of the water cycle in Iceland located at the northern NAO-pole. Water cycle extremes affect land (and sea) and are characterised by periods of dryness and wetness, both of which occur in arid and in humid climates. Notwithstanding the considerable ecological and economical impact, the corresponding atmospheric flow patterns are also of interest, in particular, when climate simulations are to be verified and future climate scenarios need to be evaluated.

Extremes are rare by definition and difficult to estimate. Different methods can be used to describe extremes. Nonparametric methods are based on percentiles or quantiles and are often used in meteorological science for the calculation of extreme indices (for example: KLEIN TANK and KÖNNEN (2003)). Parametric methods, however, enable calculations of extreme value distributions (COLES (2001)). In the following the standardised precipitation index (SPI) is applied, which has been proposed to obtain a quantitive meaning for an oth-

*Corresponding author: Klaus Fraedrich, Meteorologisches Institut, Universit¨at Hamburg, Bundesstrasse 55, D-20146 Hamburg, Germany, email: klaus.fraedrich@zmaw.de

erwise loose definition (BORDI et al. (2006)), in order to monitor dryness and wetness (MCKEE et al. (1993)). Although for the index calculation parametric methods are used, the SPI is a nonparametric method, because estimated distributions are only used for the standardisation. Therefore, the SPI may be regarded as an extension of nonparametric methods.

The goals of this paper are twofold: (a) linking extreme dryness and wetness with atmospheric flow patterns and (b) estimating future changes in the occurrence of the extremes. To achieve these aims, our analysis is structured as follows: The SPI and the observed and simulated data sets to be analysed are introduced (sections 2 and 3). Observed dryness and wetness as extremes of the SPI and the associated observed large scale atmospheric flow are identified and compared with transient 20th century model simulation (section 4). Based on this comparison dryness and wetness (and the related atmospheric flow) statistics are evaluated for future climate scenarios (section 5). A brief summary concludes the analyses (section 6). In addition, the relation between SPI extremes to cyclone track densities are investigated in the Appendix.

2 Data and model simulations

Iceland precipitation is represented by single time series in terms of monthly means of area (about $10^5 \mathrm{km}^2$) averages to make analyses of higher resolution observations and low resolution simulations comparable.

Observations: Observed Iceland precipitation values are taken from a precipitation climatology at 0.5° resolution (VASCLIMO, Variability Analysis of Surface Climate Observations, BECK et al. (2005)). The VASCLIMO dataset is very similar to the CRU TS 2.1 dataset (CRU, Climate Research Unit, MITCHELL and JONES (2005)): for area averaged Island precipitation on a monthly basis, timeseries show nearly identical distributional properties with the same variability (correlations larger than 0.9). The observed atmospheric flow is presented by the 500*hPa* geopotential height analysis (ERA40, SIMMONS and GIBSON (2000)). Both precipitation and geopotential height data sets are analysed for the overlapping period 1958 to 2000.

Simulations: The coupled atmosphere-ocean climate model is ECHAM5/MPI-OM (ROECKNER et al. (2003), MARSLAND et al. (2003)); the atmosphere is in T63 spectral resolution (about 1.8°) with 31 vertical levels. Thus Iceland is represented by 6 gridboxes. No flux correction is applied. The following model simulations are analysed:

1. Pre-industrial control experiment (CTL) with constant greenhouse gas concentrations as observed in 1860 (500 years integration).
2. Transient 20th century simulation (1860 to 2000) to compare with observations (three ensemble members).
3. Stabilisation run (20C) with greenhouse gases fixed at present day climate of the year 2000 (three 100 year ensemble members).
4. Stabilisation run (A1B) with greenhouse gases fixed at 2100 following the A1B scenario (NAKIĆENOVIĆ et al. (2000)), which represents the climate after an intermediate greenhouse gas increase (three 100 year ensemble members).

Trends: Precipitation trends from 1951 to 2000 are determined for each calendar month for both observations and the 20th century simulation. Although there is evidence of local trends in observed Iceland precipitation (BECK et al. (2005)), the area averaging removes them. Only two months show a significant trend (95% confidence level, according to Mann-Kendall-Test). Trends are not removed in the following, because calculations with and without them did not change the results.

3 Standardised Precipitation Index (SPI)

The SPI was introduced by MCKEE et al. (1993) to classify and monitor dryness and wetness. The calculation of the SPI is based on an "equal probability transformation": monthly precipitation is transformed to a standard normal distribution to yield SPI values by preserving probabilities (details are given in the Appendix of BORDI and SUTERA (2001)). The standardisation ensures, that the SPI gives a uniform measure for dryness and wetness in different climate regimes or under seasonal dependence. The SPI can be constructed for different timescales characterizing meteorological, hydrological and agricultural periods of dryness and wetness. Here we choose the monthly time scale characterising the meteorologically relevant period, that is, wet and dry spells and its extremes. The SPI classification is shown in Table 1.

Distribution: The transformation depends on the assumed statistical distribution of monthly precipitation. A false distribution type leads to systematic errors, which are most severe at the upper and lower tails and, therefore, for the extreme values. The gamma distribution, as

SPI intervals	SPI classes	P
$\mathrm{SPI} \geq 2$	W3: extremely wet	2.3
$2 > \mathrm{SPI} \geq 1.5$	W2: severely wet	4.4
$1.5 > \mathrm{SPI} \geq 1$	W1: moderately wet	9.2
$1 > \mathrm{SPI} > -1$	W0, D0: normal	68.2
$-1 \geq \mathrm{SPI} > -1.5$	D1: moderately dry	9.2
$-1.5 \geq \mathrm{SPI} > -2$	D2: severely dry	4.4
$\mathrm{SPI} \leq -2$	D3: extremely dry	2.3

Table 1: Standardised Precipitation Index (SPI) classes and corresponding event probability, P in %.

used by BORDI et al. (2006) to describe precipitation in Sicily, has lead to adequate results. However, this distribution does not hold for all months for the Iceland precipitation time series; for some months better fits can be achieved by the Weibull distribution. To still use a single unifying distribution type the "Generalised Gamma Distribution"is applied instead:

$$f(x) = \frac{d}{\Gamma(k)} b^{-dk} x^{(dk-1)} \exp\left(-\left(\frac{x}{b}\right)^{d}\right) \qquad (3.1)$$

with scale parameter b, two shape parameters d and k, and the gamma function $\Gamma(y)$. This version includes as special cases the gamma distribution (by setting $d = 1$) and the Weibull distribution (with $k = 1$). The two shape parameters make maximum likelihood estimation difficult and lead to convergence problems. Therefore, parameter estimation is performed by using the reparameterised version of the generalised gamma distribution (LAWLESS (1982)).

Changing climate: The transformation can also be used to identify possible dryness and wetness changes in terms of SPI values. The solid lines and arrows illustrate the transformation to SPI (Figure 1). For an example value $x = 20$, from a sample (X), which is gamma (Γ_1) distributed (solid curve), the transformation leads to a SPI value of approximately 1. Transforming the whole sample, X, results in standard normal distributed SPI values, with preserved probabilities, but only if the samples are indeed drawn from a Γ_1-distribution. The same transformation of a $y = x$ from another sample (Y), which is Γ_2 distributed, will lead to the same SPI value. But the "preserved" probability is now the probability of the Γ_2 distribution. Transforming the whole sample Y will not give the standard normal distribution. The probability difference between x from Γ_1 and y from Γ_2 occurs also after the transformation (difference between the two horizontal arrows). So, possible future precipitation changes are also detected and expressed in terms of the SPI by this transformation property.

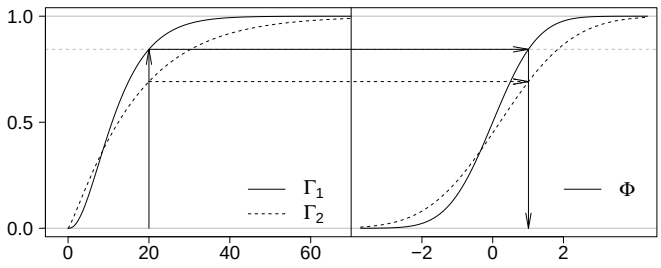

Figure 1: The transformation to SPI is illustrated by solid lines and arrows: a gamma distribution (Γ_1, left) is transformed to the standard normal distribution (Φ, right). Another gamma distribution (Γ_2, dashed lines, left) is transformed such that the probability differences remain the same on the both sides. Note that the resulting distribution (dashed lines, right) does not have the properties of the standard normal distribution (shown are cumulative distribution functions).

4 SPI extremes and atmospheric flow: present day climate

For 1958 to 2000 the observed monthly extreme SPI classes for Iceland are associated with monthly mean northern hemisphere 500*hPa* geopotential height anomaly composites to identify atmospheric flow fields related to extreme dryness and wetness. This provides the background for comparison with climate simulations.

4.1 Observations

SPI: In a first step, precipitation is transformed to SPI. The time period is short and the extreme events are rare. According to Table 1 one expects approximately 11 extreme wet and 11 dry months in 43 years. Extreme and severe SPI classes are combined to increase the sample size. Then, composite maps of the 500*hPa* geopotential height anomalies (of extreme wet and dry months) are constructed as averages over the deviations from the mean over all months of the remaining SPI classes.

Circulation: In Figure 2 the resulting geopotential height anomalies are composited for severe and extreme wet (a) and dry (b) conditions and are averaged for the whole year. In the severe and extreme wet case a negative anomaly centre is found near Greenland and a positive anomaly centre near Europe between England and Scandinavia, which are steering centres of the flow. The signs of the anomaly centres are reversed in the case of severe and extreme dry conditions, but their locations remain the same. These patterns are nearly consistent throughout the seasons, with slightly varying magnitude and location of anomaly centres (not shown). The anomalies are highest during autumn and winter, in spring and summer the anomalies are weaker. Around Greenland no deviations of the location occur throughout the seasons, whereas in the wet cases the positive anomaly centre is shifted northward in spring. In the dry cases the negative anomaly centre is split in two poles in autumn.

CASSOU et al. (2004) found four climate regimes in the winter 500*hPa* geopotential height field by cluster analysis, capturing nonlinearities of North-Atlantic weather regimes. One of the regimes (the west-east dipole between Greenland and Scandinavia, their Figure 3(d)) is similar to the wet extreme anomaly field (Figure 2 (a)). However, the dry extreme anomaly field (Figure 2 (b)) has no clear equivalent: for NAO negative (CASSOU et al. (2004) with Figure 3(a)), the positive poles over South-Greenland coincide, while the negative pole (Figure 2 (b)) is displaced north-eastward. That is, extremes can partly be associated with weather regimes, associated with cluster analysis. Therefore, NAO relations

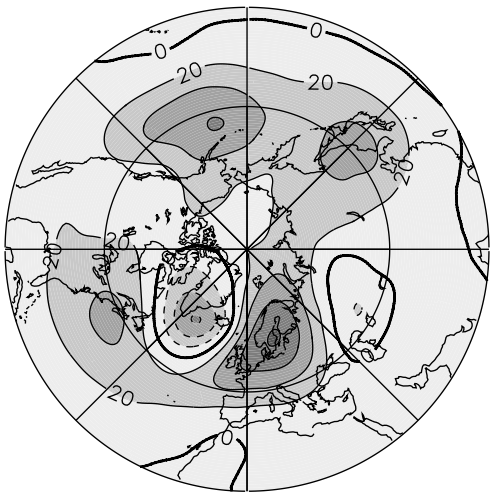

(a) Severe and extreme wet conditions

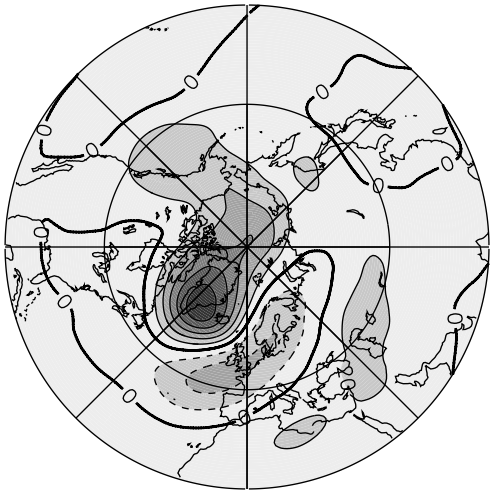

(b) Severe and extreme dry conditions

Figure 2: Composite maps of ERA40 geopotential height anomalies [gpm] corresponding to observed severe and extreme (a) wet (SPI ≥ 1.5) and (b) dry (SPI ≤ -1.5) conditions in Iceland. Continuous lines show positive and dashed lines negative anomalies. The contour intervals are $20gpm$.

with Iceland precipitation (HANNA et al. (2004)) and, possibly, cyclone activity (SERREZE et al. (1997)) could be extended in view of these results for both present day and changing climates.

In summarising, the anomalous flow patterns associated with severe and extreme wet SPI classes (Figure 2(a)) are related to an anomalous northward atmospheric flow (of warm and wet air masses) from the Atlantic region. This flow is reversed in severe and extreme dry conditions, where Iceland is under the influence of dry polar air masses. Thus, a Europe-Greenland geopotential height difference is suggested as a flow index, EGI (used in section 5), representing the pressure gradient, which characterises the anomalous circulation.

4.2 Climate model: transient simulation

Verifying climate models by comparing observations with the transient 20th century simulations (1860 to 2000) is prerequisite for evaluating the representativeness of future scenarios. Thus, the respective ensemble simulations are subjected to the same SPI and circulation pattern analysis. It should be noted that the ensemble members are not simulations of the present climate, but of scenarios starting from the pre-industrial climate forced with observed greenhouse gases until the year 2000.

SPI: Since SPI is calculated on a monthly basis, the comparison of the observed and model simulated precipitation is made for each calender month. A two-sample Kolmogorov-Smirnov test is performed testing the null hypothesis that precipitation data are drawn from the same continuous distribution (applied to each individual ensemble member). Test results are shown in Table 2 in terms of probability, p, of null hypothesis rejection: In six months (January February, June to August, October) the null hypothesis is accepted for each member; in three months (March, May and November) there is one ensemble member for which the null hypothesis is rejected, so that there is still some agreement between observation and model simulations. In September and December one ensemble member fulfils the test, while no agreement is found for April. In summarising, no single season shows a systematic departure. Best agreement exists in summer and worst in spring, possibly due to ENSO influencing the flow and cyclone track patterns (FRAEDRICH (1994)). Though not perfect, the agreement between observed and model simulated precipitation can be considered as good.

Circulation: Now the flow fields associated with severe and extreme SPI classes are determined from model sim-

Month	1	2	3
1	**0.717**	**0.272**	**0.179**
2	**0.998**	**0.549**	**0.396**
3	**0.179**	0.001	**0.068**
4	0	0.006	0.039
5	**0.717**	0.022	**0.272**
6	**0.396**	**0.272**	**0.549**
7	**0.549**	**0.179**	**0.717**
8	**0.869**	**0.396**	**0.272**
9	0.039	0.001	**0.068**
10	**0.967**	**0.869**	**0.967**
11	0.039	**0.396**	**0.272**
12	0.006	**0.272**	0

Table 2: Two sample Kolmogorov-Smirnov test: estimated p-values are shown for each ensemble member (1 to 3). The null hypothesis is rejected at 5% level for $p < 0.05$.

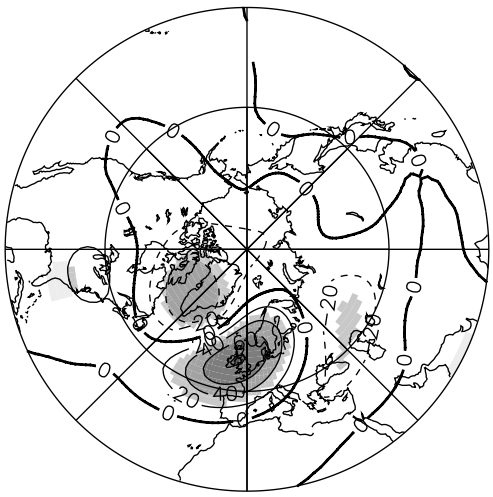

(a) Severe and extreme wet conditions

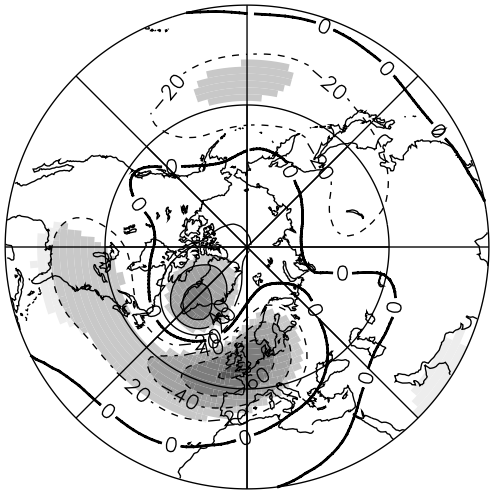

(b) Severe and extreme dry conditions

Figure 3: Composite maps of geopotential height anomalies ([gpm]) of the transient 20th century simulation corresponding to observed severe and extreme (a) wet (SPI ≥ 1.5) and (b) dry (SPI ≤ -1.5) conditions in Iceland. Contour lines see Figure 2, significant areas shaded (95% confidence level).

ulations to analyse and compare wetness and dryness related circulation patterns. All ensemble members are analysed together and the results are presented in Figure 3, where significant anomaly differences are shaded according to a T-test (95% confidence). Nearly the same anomaly patterns are found in observations and the transient simulations of the present day climate (Figures 2 and 3). Comparison shows the following results: For severe and extreme wetness the model area of significant positive geopotential height anomalies is shifted southward with the European centre near England while negative anomalies show the same strength and location. For severe and extreme dryness composites show larger deviations: positive anomalies are much stronger in the observed geopotential heights, while negative ones reach higher values in simulations. The strengths of the Greenland and Europe anomalies are asymmetric in the observations and almost symmetric in the simulations, while the centres' locations remain the same (Figure 3). Some of these differences may result from the short time period of the observations and, therefore, represent random fluctuations, or from model bias underrepresenting the tropical influence on mid-latitude weather and climate. However, the time limitation in the data series does not influence the present analysis. Only if differences were much larger than found, the model bias would have reached a magnitude that credible results of the projected future may affected. In summarising, the patterns of observed and simulated flow fields agree well and the statistical test highlights the important areas steering the flow. Furthermore, they are consistent with the previously given physical explanation.

5 Climate change scenarios

The ensemble members of two stabilisation runs are analysed representing present day (20C) and the scenario (A1B) climates and both sets are compared with the pre-industrial (CTL) climate.

SPI: The SPI classes (Figure 4) show almost no differences between present day and pre-industrial frequencies. However, the scenario climate compared with the pre-industrial shows a strong increase of severe and extreme wet conditions. The frequency of the severe wet class is more than doubled, while in the extreme wet class it is more than trebled. In all dry classes the frequencies are reduced, except for the extreme dry class, which remains unchanged. Differences in frequency between extreme SPI classes of model simulations are now evaluated on a seasonal basis (Figure 5). The present day climate shows only small changes in wet and dry extremes compared with the pre-industrial simulation. The

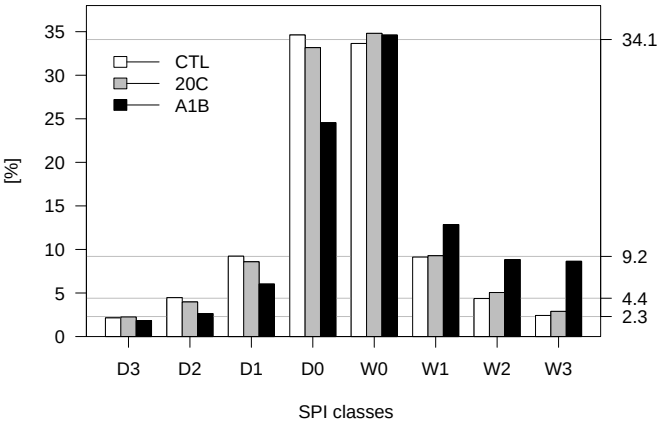

Figure 4: Frequencies of SPI classes (see Table 1): pre-industrial (CTL), present day (20C) and scenario climate (A1B); SPI event probabilities in % on right vertical axis.

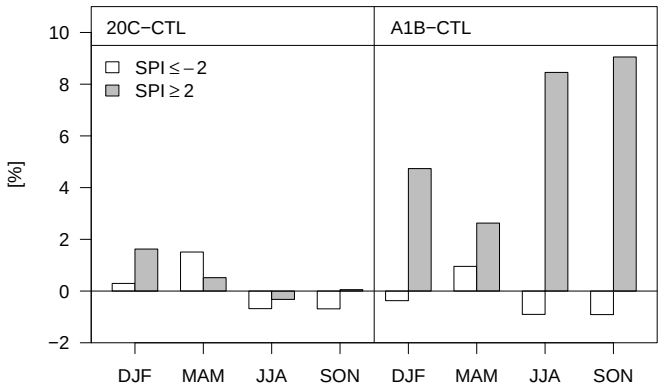

Figure 5: Differences of extreme SPI class frequencies (per season): present day (20C) minus pre-industrial (CTL) climates (left), scenario (A1B) minus pre-industrial (CTL) climates (right).

scenario climate reveals small (large) changes for the extreme dry (wet) SPI classes; note that, in the scenario climate, the increase in the wet extremes is strongest in summer and autumn; a considerable increase occurs in winter, while it is lowest for spring. Small differences between the single ensemble members are found, which lie in the range of random variations. All members show the same seasonal response.

Circulation: The SPI extremes in both pre-industrial and scenario simulations are also associated with the previously found atmospheric circulation anomalies and their steering centres (not shown). Relating the frequency increase of extreme wet SPI classes to anomalous flow patterns is analysed by the joint density distribution of the respective indices, SPI and EGI (introduced in sections 3 and 4.1). Significant positive and negative geopotential height anomalies define the steering centres of both wet or dry patterns (see Figure 3). The "wet/dry"intersections yield a dipole, whose area averaged geopotential height anomalies define the Europe-Greenland Index (EGI), that is, a difference of area averaged geopotentials between the Europe and Greenland "wet/dry" intersections. Extreme wet patterns correspond to positive EGI values with enhanced southwesterly flow and extreme dry conditions in Iceland to negative ones, with reduced southwesterly flow. This Europe-Greenland circulation index, EGI, is now related to the Iceland SPI for each season (Figure 6).

The following results are noted:

EGI-SPI correlations: In the pre-industrial (observed) climate SPI and EGI are highly correlated and the correlations range from 0.64 (0.6) in summer to 0.72 (0.69) in winter. This shows that the EGI is not only relevant for the extreme but also for the other SPI classes. The correlations remain almost unaltered in the scenario climate.

EGI-SPI joint density (pre-industrial): The joint density estimates also show that high (low) SPI values are associated with high (low) EGI values (Figure 6, left column). EGI values show larger variability in winter than in summer (see also discussion in section 2), as it is obvious from density tails. In summarising, these statistics support the introduction of EGI representing the atmospheric flow relation with SPI and its extremes (Section 4.1).

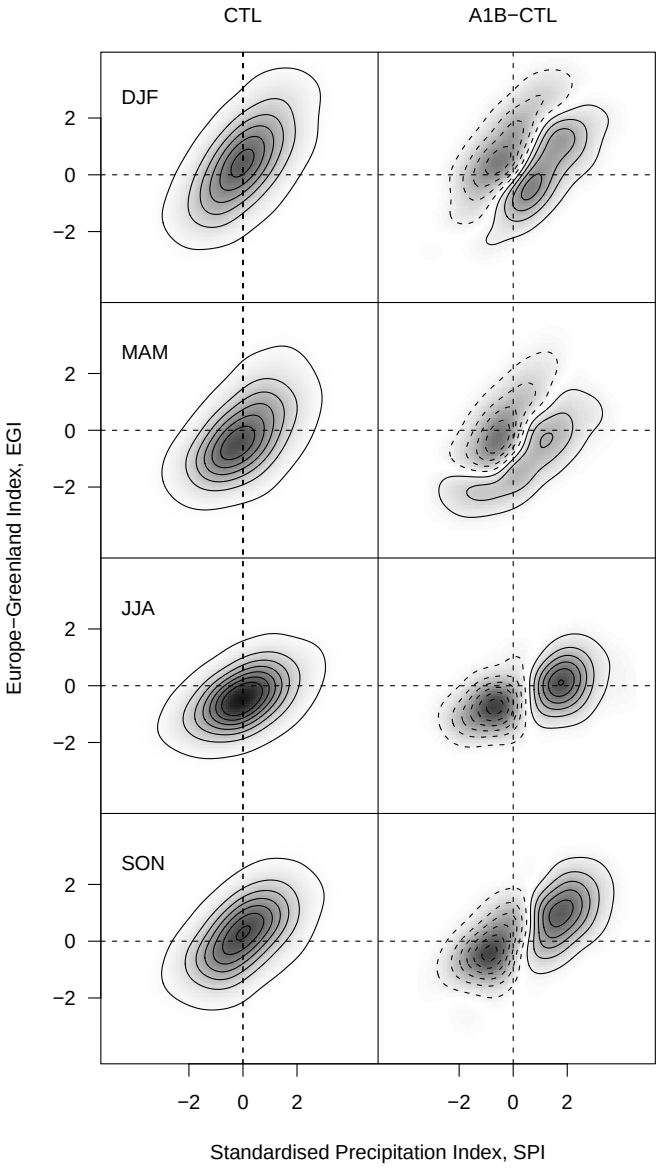

Figure 6: Seasonal joint density estimates of standardised precipitation index (SPI axis) and Europe-Greenland geopotential height difference (EGI axis in $[100gpm]$): pre-industrial climate (CTL, left) and density differences between scenario and pre-industrial climate (A1B-CTL, right). Density contours start from 0.005 with contour intervals 0.025; negative (positive) density differences are dashed (solid) starting from -0.001 (0.001) with contour intervals 0.001. Higher values are shaded darker.

EGI-SPI joint density difference (A1B and CTL): The two dimensional densities (EGI, SPI) are calculated for the scenario climate to determine the density differences

between the scenario and pre-industrial climate (Figure 6, right column). A shift along the SPI axis to higher values is obvious in all seasons. Note that the positive contour lines reach highest values (SPI ≈ 2) in summer and autumn, which is due to more extreme wet events (than in the other seasons, see also Figure 5). The shift along the EGI axis, however, is less pronounced. The change of the densities to higher EGI values is only found in summer and autumn, i.e. the wet pattern (Figures 2(a) or 3(a)) occurs more often and higher differences between the poles are getting more probable. This is reversed in winter and spring, where the density is reduced for high positive EGI values. In these seasons the occurrence of the dry pattern (Figures 2(b) or 3(b)) has an increased probability. Note, that all individual ensemble members show the same response, as in Figure 6, with nearly no differences.

In summarising, we conclude that (i) the increase of extreme wet events (Figure 5) in winter and spring (of the A1B scenario climate) is *not* a result of an intensification of the anomaly flow pattern. That is, because the density of high EGI values decreases while the density of high SPI values increases. As the relation between EGI and SPI is still present in the scenario climate, the noted SPI increase in the scenario must result from another mechanism as, for example, moisture rising in a warmer climate. (ii) The seasonal variability of extreme wet SPI frequency changes (A1B-scenario minus CTL-control, Figure 5) are related to EGI (or flow pattern) density changes (A1B-CTL, 6). That is, the largest extreme wet SPI frequency increase occurs in summer and autumn, which corresponds to the increasing density of positive EGI or, to higher EGI values occurring more often (see anomaly pattern in Figure 3 (a)). In addition, extreme wet SPI frequencies rising less in spring than in winter (Figure 5) is consistent with a stronger decrease of density of positive EGI.

6 Summary and conclusions

Extremes of dryness and wetness in Iceland are analysed in terms of the standardised precipitation index (SPI). Observed geopotential height anomalies composited about extreme SPI events show a dipole like structure representing steering centres over Europe's westcoast and Greenland's South. The Europe-Greenland Index (EGI) of geopotential height differences reverses sign from wet to dry events. The analysis of observations is compared with transient 20th century (ensemble) simulations followed by the same analysis of the future A1B-scenario. Some results are summarised:

1. Agreement between observed and simulated transient 20th century precipitation (SPI) statistics can be considered as good and the observed SPI-circulation relation is also found in the simulation.
2. No significant differences appear in the frequencies of the monthly SPI classes (per year) and monthly SPI extremes (per season) between present day climate (20th century stabilisation runs) and pre-industrial (CTL) simulation.
3. Significant and large differences occur in the frequencies of the severe and the extreme wet SPI classes between scenario (A1B) climate (21st century stabilisation runs) and the pre-industrial (CTL) climate (stabilisation runs).
4. Extreme wet SPI frequencies increase in winter and spring of the scenario climate. This is not a result of intensifying flow anomalies but may be related to other mechanisms as, for example, moisture rising in a warmer climate.
5. But, the seasonally differing responses in scenario frequencies (of extreme wet SPI classes) are consistent with the changing anomalous flow pattern.

These analyses add information to Iceland climate studies introducing monthly precipitation extremes in terms of dryness and wetness and their possible link to an atmospheric circulation pattern steered by geopotential height anomalies over Greenland and Europe. New are the methods introduced for analysing extremes under changing climate conditions and linking this with the associated atmospheric flow pattern. However, to aid decision making based on future scenarios requires test and analysis of other climate change scenarios and different climate models. Extension to other regions governed by different circulation regimes and climates will be presented in due course.

Acknowledgements

Support by the EU-Nest project E2-C2 is acknowledged (for F. Sienz); the link to SFB-512 gives the background for this analysis (K. Fraedrich). Thanks to Jürgen Grieser for fruitful discussions and Frank Lunkeit for comments on the manuscript. The R DEVELOPMENT CORE TEAM (2005) is acknowledged for providing the statistics package "R". The authors would also like to thank the reviewers for their comments on the manuscript.

Appendix: Cyclone density analysis

This appendix presents results of cyclone tracking analysis applied to spells of wetness and dryness in Iceland. The tracking algorithm is applied as described in detail by SCHNEIDEREIT et al. (2007) (see also references therein) with two exceptions: the minimum cyclone lifetime is 48 hours and their minimum travel distance is 1000 km. The winter season is considered. Cyclone densities for wet extremes (Figure 7(a)) show enhanced magnitude near 60° North with a southwest-northeast

orientation along the Greenland trough anomaly and its largest gradient. The pattern is similar to the winter mean density. For dry conditions (Figure 7(b)) cyclone activity is enhanced and more zonally oriented along 50° North.

In addition, cyclone density change is presented for scenario (A1B) minus transient 20th century simulation. For extreme wet conditions (SPI ≥ 1.5) the density is strongly reduced in Norwegian-Barents Sea (up to -10%, Figure 7(c)), consistent with the reduced EGI (Figure 6, top right panel). That is, the increasing SPI change in Iceland (section 5) cannot be related to an increasing number of cyclones.

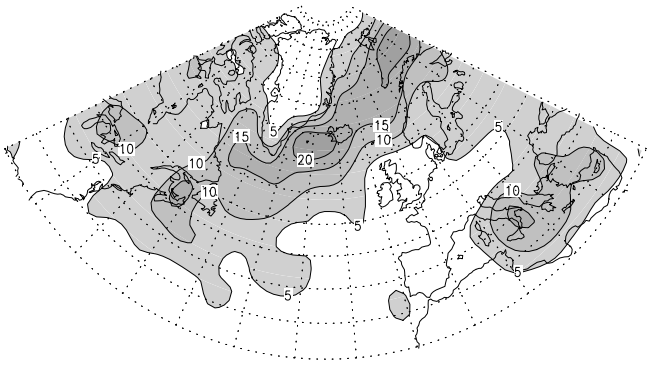

(a) Transient 20th century: severe and extreme wet conditions

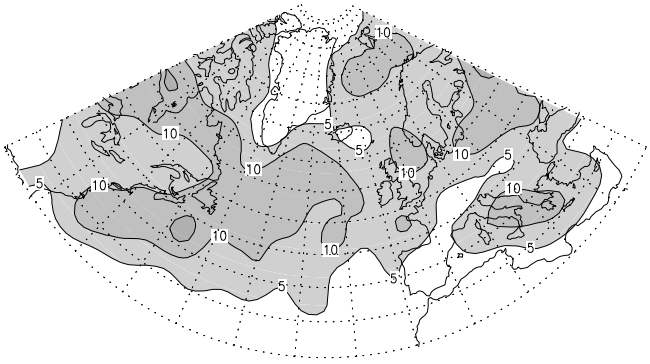

(b) Transient 20th century: severe and extreme dry conditions

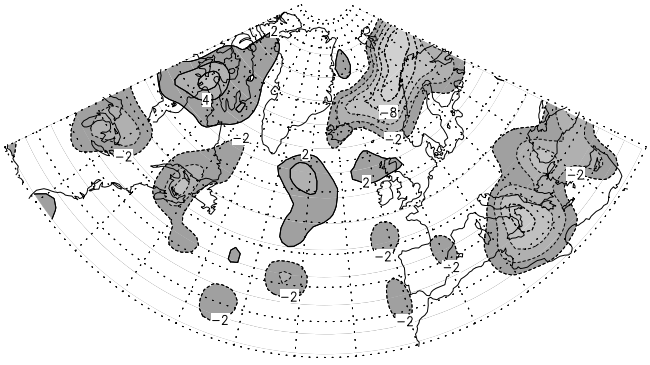

(c) Scenario minus transient 20th century: cyclone density change

Figure 7: Cyclone densities of the transient 20th century simulation in winter (DJF, 1950- 2000) corresponding to observed severe and extreme (a) wet (SPI ≥ 1.5) and (b) dry (SPI ≤ -1.5) conditions in Iceland. The contour intervals are 5%. (c) Mean cyclone density change between scenario (A1B) and transient 20th century simulation climate for severe and extreme wet conditions. Continuous lines show positive and dashed lines negative differences, with contour intervals of 2%.

References

BECK, C., J. GRIESER, B. RUDOLF, 2005: A new monthly precipitation climatology for the global land areas for the period 1951 to 2000. Climate status report 2004, German Weather Service, Offenbach, Germany, 181 - 190.

BORDI, I., K. FRAEDRICH, M. PETITTA, A. SUTERA, 2006: Extreme value analysis of wet and dry periods in Sicily. Theor. Appl. Climatol. (in press) .

BORDI, I., A. SUTERA, 2001: Fifty years of precipitation: Some spatially remote teleconnections. Water Resour. Manag. **15**, 247–280.

CASSOU, C., L. TERRAY, J. W. HURRELL, C. DESER, 2004: North Atlantic winter climate regimes: spatial asymmetry, stationarity with time, and oceanic forcing. J. Clim. **17**(5), 1055–1068.

COLES, S., 2001: An Introduction to Statistical Modeling of Extreme Values. Springer-Verlag, 207 pp.

FRAEDRICH, K., 1994: ENSO impact on Europe? - A review. Tellus **46A**, 541–552.

HANNA, E., T. JÓNSSON, J. E. BOX, 2004: An analysis of Icelandic climate since the nineteenth century. Int. J. Climatol. **24**(10), 1193–1210.

KLEIN TANK, A. M. G., G. P. KÖNNEN, 2003: Trends in indices of daily temperature and precipitation extremes in Europe, 1946-99. J. Clim. **16**(22), 3665–3680.

LAWLESS, J. F., 1982: Statistical Models and Methods for Lifetime Data. John Wiley & Sons, Inc., New York, 580 pp.

MARSLAND, S. J., H. HAAK, J. H. JUNGCLAUS, M. LATIF, F. RÖSKE, 2003: The Max-Planck-Institute global ocean/sea ice model with orthogonal curvilinear coordinates. Ocean Model. **5**(2), 91–127.

MCKEE, T. B., N. J. DOESKIN, J. KLEIST, 1993: The relationship of drought frequency and duration to time scales. In 8th Conf. on applied climatology, American Meteorological Society, Anaheim, Canada, 179–184.

MITCHELL, T. D., P. D. JONES, 2005: An improved method of constructing a database of monthly climate observations and associated high-resolution grids. Int. J. Climatol. **25**(6), 693–712.

NAKIĆENOVIĆ, N. J., et al., 2000: IPCC Special Report on Emissions Scenarios. Cambridge University Press, Cambridge, United Kingdom and New York, USA.

R DEVELOPMENT CORE TEAM, 2005: R: A language and environment for statistical computing. R Foundation for Statistical Computing, Vienna, Austria, URL `http://www.R-project.org`.

ROECKNER, E., et al., 2003: The atmopheric general circulation model ECHAM5, part 1: Model description. Report 349, Max-Planck-Institut for Meteorology, Hamburg, Germany, 127 pp.

SCHNEIDEREIT, A., R. BLENDER, K. FRAEDRICH, F. LUNKEIT, 2007: Iceland climate and North Atlantic cyclones in ERA40 reanalysis. Meteorol. Z. (this issue) .

SERREZE, M. C., F. CARSE, R. G. BARRY, J. C. ROGERS, 1997: Icelandic low cyclone activity: climatological features, linkages with the NAO, and relationships with recent changes in the northern hemisphere circulation. J. Clim. **10**(3), 453–464.

SFB-512, 2005: Cyclones and the North Atlantic climate system. Meteorol. Z. **14**(6), 693–821.

SIMMONS, A. J., J. K. GIBSON, 2000: The ERA40 project plan. ERA40 Report Series 1, European Center for Medium-Range Weather Forcasts, Reading, United Kingdom, 66 pp.